ChemComm

ROYAL SOCIETY OF CHEMISTRY

FEATURE ARTICLE

View Article Online
View Journal | View Issue

Cite this: *Chem. Commun.*, 2025, **61**, 658

Built-in electric field guides oxygen evolution electrocatalyst reconstruction

Chunmei Ni,[a] Kun Wang,[a] Lei Jin,[a] Yang Liu,[a] Jie Chen,[a] Lida Yang,[a] Chanyuan Ji,[a] Hui Xu, *[a] Zhao Li *[ab] and Lin Tian *[a]

Received 13th September 2024,
Accepted 25th November 2024

DOI: 10.1039/d4cc04740k

rsc.li/chemcomm

Creating a built-in electric field (BIEF) in catalysts represents an effective strategy to promote electron transfer and induce asymmetric charge distribution, thereby facilitating surface dynamic reconstruction under oxygen evolution reaction (OER) conditions. This review summarizes recent advancements in the field of OER electrocatalysts, with a focus on regulating the work function of components to tailor the BIEFs to guide surface reconstruction processes. It also discusses the importance of surface reconstruction in improving electrocatalytic performance and the influence of BIEFs on the reconstruction of catalysts. By analyzing various strategies for manipulating electric fields for guiding surface reconstruction of OER electrocatalysts, along with numerous representative examples, this review highlights how these techniques can enhance catalytic activity and stability. The findings underscore the potential of engineered BIEFs as a powerful tool in the design of next-generation electrocatalysts, paving the way for more efficient energy conversion technologies.

1. Introduction

Compared to traditional methods such as coal gasification, steam methane reforming, and mineral fuel pyrolysis for hydrogen production, the water electrolysis technique is simple, offers high gas purity, and has broad application prospects.[1,2] Electrocatalytic water splitting involves the anodic oxygen evolution reaction (OER) and the cathodic hydrogen evolution reaction (HER).[3] Compared to the two-electron transfer process of the HER, the OER is a complex multi-step proton-coupled electron transfer process, whose reaction kinetics are slow, thus severely limiting the efficiency of the cathodic HER by the anodic OER.[4–9] Therefore, designing efficient OER electrocatalysts to reduce the high overpotential of water splitting has become a research hotspot in recent years.

Noble metal oxides such as IrO_2 and RuO_2 are benchmark catalysts for the OER, occupying the top positions in the volcano plot of OER activity.[10,11] However, their high cost, scarcity, and susceptibility to dissolution at high anodic potentials (>1.6 V) significantly limit the large-scale application of water electrolysis for hydrogen production.[12–14] Compounds based on 3d transition metals, such as Ni, Fe, and Co catalysts, are promising replacements for noble metal catalysts due to their abundant crustal reserves.[15,16] However, during the electrocatalytic OER process, the surface structure and composition of 3d transition metal compounds dynamically change, leading to unclear catalytic mechanisms.[17–19] With the development of *in situ* characterization techniques, researchers have found that catalysts undergo surface reconstruction in alkaline electrolytes accompanied by an increase in oxidation state, resulting in the formation of more catalytically active reactive species.[20–22] As a chemical reaction occurring on the electrode surface, the quantity and activity of the reactive species generated are impacted by the activation conditions and the properties of the catalyst.[23–25] Regulating the reconstruction process to produce a large number of highly active species has been confirmed as an effective strategy to enhance the OER performance of catalysts.[26–28]

The reconstruction process of electrocatalysts under OER conditions is often accompanied by an increase in the valence state of metal ions and the formation of corresponding oxides or hydroxyl oxides.[29,30] The reconstruction of pre-catalysts leads to the formation of truly active sites. Modification and control strategies based on surface activation, defect engineering, dissolution etching, ion doping, and heterostructure construction can regulate the phase and electronic structure of pre-catalysts, increase electron transfer rates, and reduce the energy barrier required for the formation of active species, thereby improving the reconstruction rate and degree of catalysts in the OER process.[31–34] Although significant research progress has been made in surface reconstruction and a basic understanding of

[a] *Key Laboratory of Advanced Catalytic Materials and Technology, Advanced Catalysis and Green Manufacturing Collaborative Innovation Center, Changzhou University, Changzhou, Jiangsu Province 213164, China.*
E-mail: xuhui006@cczu.edu.cn, xzitlz@xzit.edu.cn, xzittl@xzit.edu.cn
[b] *School of Materials and Chemical Engineering, Xuzhou University of Technology, Xuzhou, 221018, P. R. China*

surface reconstruction has been established, there are still many urgent issues that need to be addressed, such as the regulatory mechanism, the impact of the degree/depth of surface reconstruction on catalytic activity, and the influence of reconstruction on the electrochemical stability. Therefore, corresponding regulatory strategies should be developed to boost the formation of highly active species while inhibiting the dissolution of these active substances without significantly affecting the reconstruction process.

In recent years, research on the construction and regulation of built-in electric fields (BIEF) in catalysts has been of great significance for promoting electron transfer, enhancing intrinsic activity, and mediating surface reconstruction.[35–37] Research has shown that electron transfer derived from BIEF directly affects the charge density around the active centre, regulates the electronic structure of the catalyst, and enhances intrinsic activity.[38–40] Meanwhile, the coexistence of electron-rich and electron-deficient regions is beneficial for increasing the concentration of reactants in the local microenvironment of multiphase interfaces, optimizing the adsorption and desorption of OER intermediates, and improving the reaction rates and activity. In the electron-deficient region, strong OH^- adsorption not only enhances mass transfer but also suppresses changes in the local reaction microenvironment, improving the stability of the catalyst.[41,42] Therefore, constructing a BIEF and tailoring the asymmetric distribution of electrons can precisely regulate the surface reconstruction of catalysts, generate a large number of highly active reactive species, and further enhance the electrocatalytic OER activity and stability.

Aiming to provide guidance for the further development of more advanced OER electrocatalysts, this timely review summarizes the recent advances in tailoring the BIEF to guide the surface dynamic reconstruction of OER electrocatalysts. This review focuses on the reconstruction phenomena and advanced characterizations, and also systematically discusses the various strategies for tailoring the BIEF to guide the reconstruction (Scheme 1). In addition, we also generalize a series of typical examples to highlight the great influence of BIEF on the reconstruction process of OER electrocatalysts. Through this review, we hope to provide insights into the design and preparation of reconstructed electrocatalysts for the benefit of readers that are interested in the field of electrocatalysis.

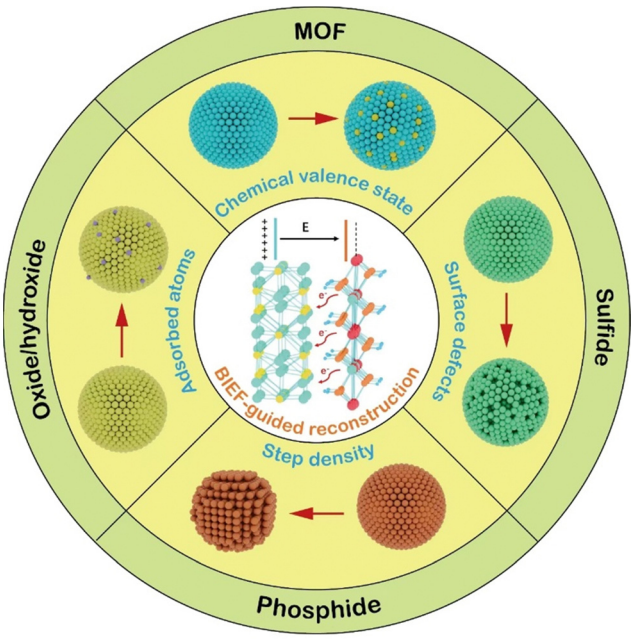

Scheme 1 Schematically illustrating the regulation strategies for guiding the surface reconstruction of various catalysts.

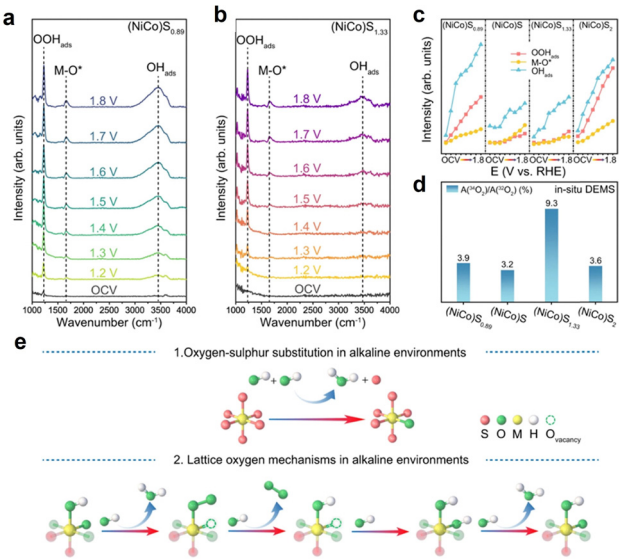

Fig. 1 (a) and (b) *In situ* FT-IR spectra of $(NiCo)S_{0.89}$ and $(NiCo)S_{1.33}$. (c) Signal strength variation diagram of characteristic FT-IR peaks of OOH_{ads}, M–O* and OH_{ads}. (d) The ratio of the LOM pathway. (e) Schematic diagram of the LOM mechanism with a lattice sulfur–oxygen substitution process. Reproduced with permission of ref. 45 copyright 2023, Nature Publishing Group.

2. Reconstruction of electrocatalysts

2.1. Reconstruction phenomena

In the electrochemical process, the surface sites of electrocatalysts have dynamic characteristics and can trigger the occurrence of reconstruction phenomena.[43] In particular, in the OER process, reconstruction can link the surface of the electrocatalyst with the active sites involved in the reaction. Surface reconstruction can also regulate the behavior of electrocatalysts such as adsorption, activation, and desorption, which in turn affects OER performance.[44] For example, Xi and coworkers discover that the lattice sulfur atoms on the surface of $(NiCo)S_{1.33}$ particles are partially replaced by oxygen in the electrolyte, inducing the formation of $(NiCo)O_xS_{1.33-x}$ with lattice oxygen sulfur coexistence (Fig. 1a–d).[45] Surface reconstructed $(NiCo)O_xS_{1.33-x}$ can significantly increase the proportion of lattice oxygen oxidation mechanism (LOM) in the sulfide matrix and reduce the generation energy barrier of NiCoOOH (Fig. 1e).

To be specific, the surface reconstruction in electrocatalysts refers to the structural changes that occur in the catalyst

material during electrochemical reactions. These changes can enhance or diminish the catalytic activity. The dynamic reconstruction of catalysts refers to the surface reconstruction, phase transformation, and dissolution and re-deposition,[46,47] which can be evaluated in terms of triggering conditions, reconstruction rate, and conversion degree. Triggering conditions refers to the potential, such as temperature, electrolyte concentration and overpotential, at which reconstruction occurs. It is well known that the presence of specific ions can promote or inhibit reconstruction, and a higher temperature can accelerate atomic mobility and facilitate the structural changes. Also, the electrochemical potential can drive the reconstruction process, affecting the stability and activity of the catalyst.

The influence of various conditions on the OER, such as the pH of electrolyte, applied potential, and temperature, on the initiation potentials and kinetics of surface reconstruction is well recognized. Notably, it is widely accepted that surface reconstruction is more likely to occur in alkaline electrolytes with high pH values.[48] This phenomenon can be attributed to the susceptibility of transition metal-based electrocatalysts to corrosion and degradation under strong acidic oxidation environments. In acidic electrolytes, the reconstruction of electrocatalysts may involve interactions between protons and active sites on the catalyst surface, resulting in changes to the composition and structure of the catalyst. Consequently, noble metals like Ir are commonly employed as catalysts for the acidic OER due to their relatively long lifespan in the harsh, corrosive conditions characteristic of acidic electrolytes. For example, Ir-based perovskites have been explored as outstanding electrocatalysts for acidic OER conditions (specifically in 0.1 M $HClO_4$). As reported by Xu *et al.*,[49] during OER testing, the Ir in the $SrCo_{0.9}Ir_{0.1}O_{3-\delta}$ catalyst transformed into highly active IrO_xH_y species, characterized by a corner-shared IrO_6 octahedron structure and an increased oxidation state (from Ir^{3+} to Ir^{5+}), while Sr and Co leached into the electrolyte. Notably, the intrinsic activity of Ir in the reconstructed IrO_xH_y was found to be more than double that of Ir in IrO_2, as demonstrated by a higher turnover efficiency.

The primary driving force behind reconstruction through various strategies is predominantly attributed to the surface chemical reactions or conversions (excluding partial dissolution), which frequently lead to the formation of new electrocatalytically active species.[50] To facilitate the reconstruction, catalysts can be designed with a high surface area to boost surface activation, optimize structural features (for example, through defect engineering), or achieve superior electronic and ionic transport properties (achieved *via* ionic doping or heterostructure development).[51,52] However, these strategies may yield varying reconstruction outcomes, as they target modifications of distinct properties of the pre-catalysts. Consequently, they can exert different influences on the kinetics, pathways, and degrees of reconstruction.

2.2. Advanced characterizations of reconstruction

Information on reconstruction can be obtained through a series of *ex situ* and *in situ* electron microscopic, *in situ* and *operando* spectra, and electrochemical tests. *In situ* electron microscopy can capture the dynamic changes of catalysts during the reaction process by observing samples in specific reaction environments, such as atmosphere, temperature, and voltage.[53] The commonly used *in situ* electron microscopy techniques include transmission electron microscopy (TEM) and scanning electron microscopy (SEM). *In situ* electron microscopy can reveal the dynamic reconstruction mechanism of catalysts under reaction conditions, including the adaptability of catalysts and the formation of intermediates. It is well documented that catalysts may self-adjust according to changes in the reaction environment during the reaction process to optimize their catalytic performance.[54,55] In addition, the *in situ* electron microscopy can capture the instantaneous state of intermediates in catalytic reactions, helping to understand the mechanism of catalytic reactions.[56,57] For example, Zhu *et al.* reported a surface dependent reconstruction phenomenon that occurs during the OER process, which demonstrated that this reconstruction process can significantly improve the OER activity of nickel (oxy)hydroxides.[58] The *ex situ* study after the OER reveals β-$Ni(OH)_2$ restructuring at the edge facets, resulting in the formation of nanoporous $Ni_{1-x}O$, which is deficient in Ni and contains Ni^{3+} species. *Operando* liquid TEM (Fig. 2a–f) and Raman spectra (Fig. 2g–i) further elucidate the crucial role of the intermediate β-NiOOH phase in both OER catalysis and the formation of $Ni_{1-x}O$, delineating the complete surface restructuring pathway. This surface restructuring is demonstrated to significantly increase the exposure of active sites, accelerate the oxidation kinetics of Ni, and optimize the bonding energy of *OH intermediates, leading to remarkable enhancements in OER activity, approximately 16-fold (Fig. 2j).

In situ spectroscopy technology reveals multiple aspects of catalyst reconstruction by real-time monitoring of changes in

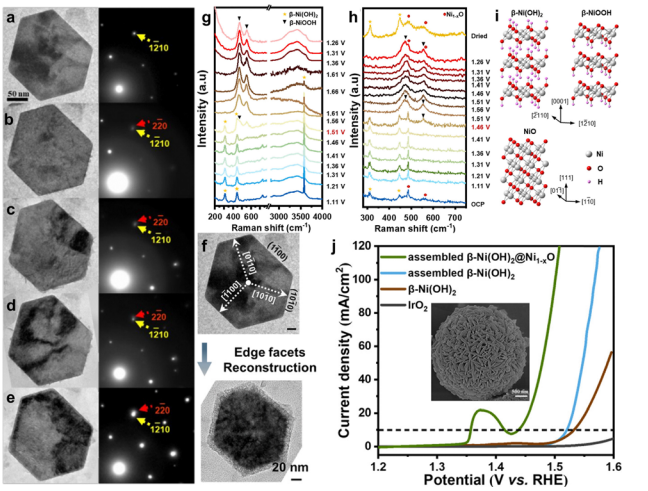

Fig. 2 *Ex situ* TEM and SAED patterns on β-$Ni(OH)_2$ (a) in the pristine state and after (b) 100, (c) 200, (d) 500, and (e) 1000 CV cycles. (f) The *operando* Raman spectra on (g) pristine β-$Ni(OH)_2$ and (h) reacted β-$Ni(OH)_2$@$Ni_{1-x}O$ after 1000 CV cycles. (i) Atomic structure of β-$Ni(OH)_2$, β-NiOOH, and NiO. (j) OER polarization curves of various catalysts. Reproduced with permission of ref. 58 copyright 2024, American Chemical Society.

the catalyst during the reaction process. As is well-known, *in situ* spectroscopy can directly observe the surface state and chemical environment of the catalyst during catalytic reactions, providing dynamic information about catalyst reconstruction.[59] Through techniques such as Raman spectroscopy, infrared spectroscopy, X-ray photoelectron spectroscopy (XPS), and X-ray absorption spectroscopy (XAS), researchers can analyze the presence and changes of different chemical species on the catalyst surface, revealing the formation of different phases during the reconstruction process. By monitoring the changes in active sites on the catalyst surface, *in situ* spectroscopy can reveal how reconstruction affects the activity of the catalyst.[60] For example, reconstruction may result in more active sites being exposed, thereby improving catalytic efficiency. *In situ* spectroscopy provides information that helps to gain a deeper understanding of the mechanism of catalytic reactions, including the formation and consumption of reaction intermediates, as well as the dynamic changes of catalysts during the reaction process.[61] Therefore, *in situ* spectroscopic techniques provide important experimental evidence for studying catalyst reconstruction, helping scientists optimize catalyst design and improve catalytic performance. For example, Oh *et al.* combined *in situ*/*Operando* XAS and Raman spectroscopy to reveal changes in phase and spin states, proposing a new electrode manufacturing strategy (Fig. 3a and b).[31] In their contribution, cobalt foam (CF) was modified by S and Fe to maintain the CoOOH phase and intermediate-spin (IS) state of the Co electrode under OER conditions. The changes in spin state of the Co electrode under OER conditions were observed by *in situ*/*operando* Raman spectroscopy (Fig. 3c–e) and X-ray absorption fine spectroscopy (XAFS) (Fig. 3f–h). Under OER conditions, the prepared CF electrode transitions from a low spin (LS) state to an IS state and remains in that state, which brings excellent OER performance.

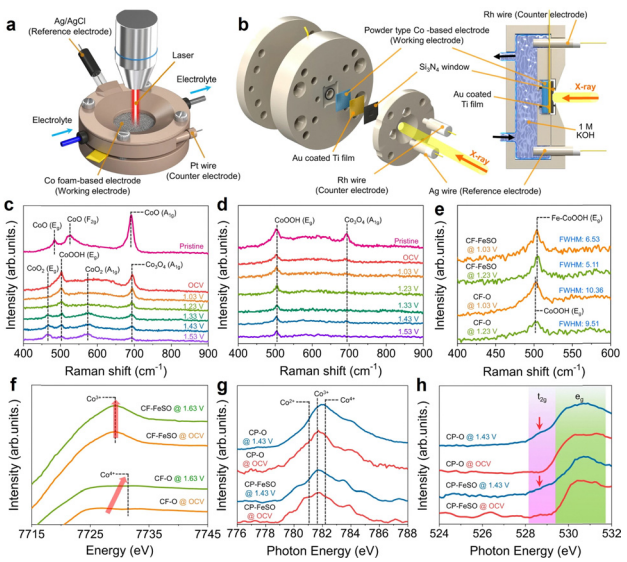

Fig. 3 Schematically showing the *in situ*/*operando* (a) Raman spectroscopy setting and (b) NEXAFS setup. (c) *In situ*/*operando* Raman spectrum of the CF-O electrode. (d) *In situ*/*operando* Raman spectrum of the CF-FeSO electrode. (e) *In situ*/*operando* Raman spectrum of the CF-based electrode for comparing the CoOOH peak. (f) *In situ*/*operando* Co K-edge XANES spectra of the CF-O and CF-FeSO electrodes. (g) *In situ*/*operando* Co L-edge NEXAFS spectra and (h) O K-edge NEXAFS spectra of the CP-O and CP-FeSO catalysts. Reproduced with permission of ref. 31 copyright 2022, Nature Publishing Group.

Moreover, electrochemical testing can characterize the reconstruction of catalysts through various methods, including cyclic voltammetry (CV), chronoamperometry (CP), electrochemical impedance spectroscopy (EIS), and linear sweep voltammetry (LSV). By measuring the relationship between current and voltage through CV, we can observe the redox behavior of the catalyst at different potentials and thus analyze the active sites and reconstruction process of the catalyst. The CP test can evaluate the stability and reconstruction of the catalyst during the reaction process. In regard to the EIS, by applying a small amplitude of AC voltage, measuring the response of current, and analyzing the charge transfer impedance and electrolyte interface characteristics of the catalyst, researchers can understand the reconstruction process of the catalyst. Furthermore, by linearly changing the potential and measuring the current response, it is possible to provide information on the reaction kinetics of the catalyst at different potentials, which helps to understand the reconstruction mechanism. Through these electrochemical testing methods, researchers can gain a deeper understanding of the reconstruction behavior of catalysts during the reaction process, thereby optimizing their performance. By combining electrochemical testing with *in situ* characterization techniques, the structural changes and reconstruction process of the catalyst can be observed in real time. For instance, Wang and coworkers have combined the electrochemical tests and *in situ* characterization techniques to reveal the dynamic evolution of oxygen vacancies (V_O) in the Co_3O_4 (Fig. 4a).[62] *Operando* EIS (Fig. 4b–e) and CV curves indicate that at relatively low applied potentials, V_O can promote the pre-oxidation of low valence Co (Co^{2+}, partially Co^{2+} induced by V_O to balance charges). This observation confirms that V_O induces surface reconstruction of V_O–Co_3O_4 before the OER process occurs. Moreover, the results of quasi *operando* XPS and *operando* XAFS further demonstrate that the oxygen vacancies in V_O–Co_3O_4 are first filled with OH*, promoting the pre-oxidation of low-valent Co and the reconstruction/deprotonation of intermediate Co–OH*. This research work observed the structure–activity relationship between defective electrocatalysts and catalytic activity through various *in situ*/*quasi in situ* characterization techniques, revealing the dynamic evolution process of the structure of V_O–Co_3O_4 during the electrocatalytic OER. This discovery will inspire researchers to pay more attention to the relationship between the structural dynamic evolution and intrinsic activity of defective electrocatalysts, providing some references for designing more efficient catalysts.

Overall, *in situ* electron microscopy and *in situ*/*operando* spectroscopy provide high-resolution imagery and detailed chemical insights, respectively, but face limitations in replicating real electrochemical environments and complex data analysis, respectively. Electrochemical tests, while straightforward and directly tied to catalytic performance, may not offer the

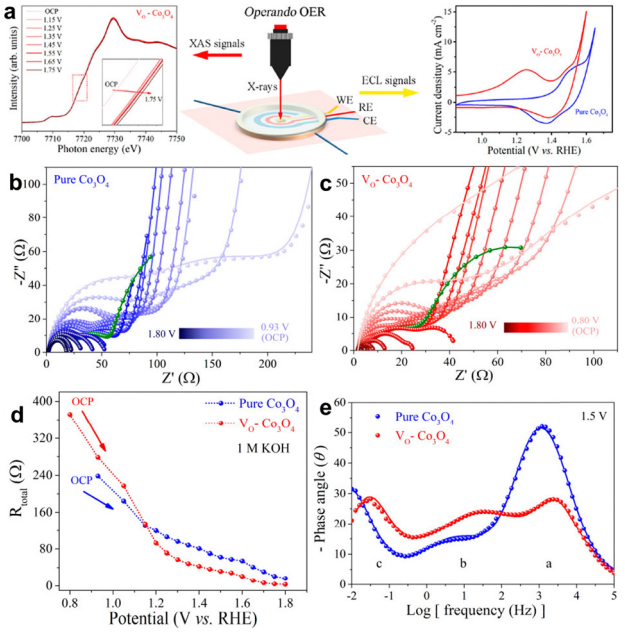

Fig. 4 (a) Schematic illustration of the combination of *operando* XAS and CV test for revealing the dynamic reconstruction of V_O–Co_3O_4. Nyquist plots for (b) pure Co_3O_4 and (c) V_O–Co_3O_4 catalysts at different applied potentials in 1 M KOH. (d) Response of the total charge transfer resistance (R_{total}) to the applied potential of Co_3O_4 samples. (e) Bode phase plots of pure Co_3O_4 and V_O–Co_3O_4 at 1.5 V *vs.* RHE in 1 M KOH. Reproduced with permission of ref. 62 copyright 2020, American Chemical Society.

detailed structural perspective necessary to fully understand surface reconstruction. Utilizing a combination of these techniques can provide a more comprehensive understanding of surface dynamics during electrocatalytic processes, helping to bridge the gaps inherent to each method.

3. Fundamentals of a built-in electric field

3.1. Definition of a built-in electric field

The formation of a BIEF is commonly related to the charge redistribution caused by the spontaneous flow of electrons at the interface. Generally speaking, when two different materials (A and B, at least one of which is a semiconductor) are in close contact, the difference in energy bands can cause interface polarization, resulting in a potential difference.[63,64] The existence of a potential difference will drive electrons near the interface to move in a directional manner until the Fermi levels on both sides are level. The simultaneous occurrence of electron-rich regions and positively charged regions leads to a gradient in charge distribution, resulting in a BIEF, which points from material A with lower work function to material B with higher work function.[65,66] The electron transfer driven by the BIEF directly affects the charge density around the active center, thereby enhancing intrinsic activity. The coexistence of electron-rich and electron deficient-regions is beneficial for increasing the concentration of reactants at the local microenvironment of the reaction interface, thereby improving the reaction rate and overall reaction activity.[67,68]

Furthermore, the electric field effect induced by the heterointerface can facilitate the asymmetric distribution of charges. In the electron-rich region of the BIEF, delocalized electrons create an electronic barrier for metal sites, which mitigates excessive losses during intense oxidation and redox reactions, thereby slowing down reconstruction processes.[69] Conversely, in the electron-deficient region, strong adsorption of OH^- not only enhances mass transfer but also stabilizes the local reaction microenvironment, improving the stability of catalyst.[70] For instance, Peng and colleagues successfully developed a tunable Ni–$FeWO_4$@WO_3/NF self-supporting electrode that exhibited efficient and stable OER performance in a neutral medium.[71] Within the BIEF of the heterojunction, WO_3 serves as an electron donor, supplying electrons to the Fe sites in tungstate while simultaneously promoting the adsorption of OH^- on the electrode surface (Fig. 5a–c), thus accelerating the mass transport. Additionally, by tailoring the work function of Ni–$FeWO_4$, the electron-deficient state of WO_3 can be altered, leading to an asymmetric distribution of interface charges within the BIEF (Fig. 5d and e). This regulation effectively suppresses the leaching of Fe and stabilizes the active hydroxyl oxides generated during neutral OER (Fig. 5f and g). Therefore, constructing an internal electric field and fine-tuning the asymmetric distribution of electrons enables precise regulation of catalyst surface reconstruction, generating numerous highly

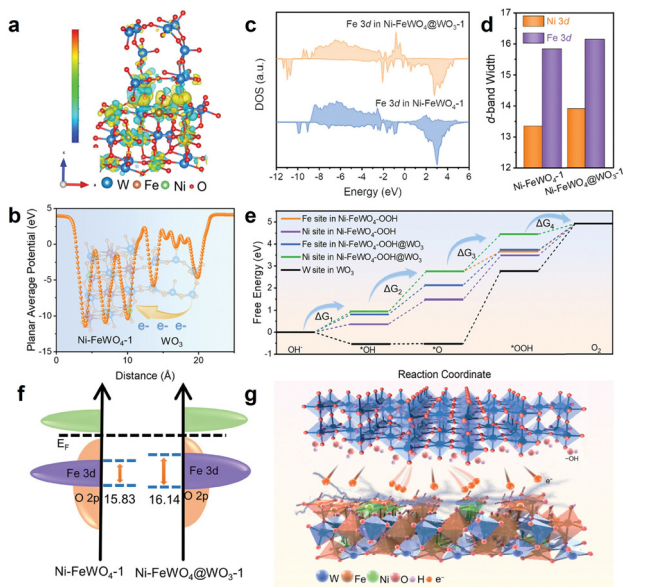

Fig. 5 (a) Charge density difference of Ni–$FeWO_4$@WO_3-1. (b) Plane-average electron difference diagram of the interface between Ni–$FeWO_4$@WO_3-1. (c) Projected DOS of Fe 3d in Ni–$FeWO_4$-1 and Ni–$FeWO_4$@WO_3-1. (d) The d-band widths of Fe 3d and Ni 3d in Ni–$FeWO_4$-1 and Ni–$FeWO_4$@WO_3-1. (e) Free energy profiles of different OER intermediates at 0 V for the Fe site. (f) Variation of the d-band widths of Fe 3d. (g) Schematic illustration of the electron barrier layer for the protection of Fe and Ni sites in Ni–$FeWO_4$@WO_3. Reproduced with permission of ref. 71 copyright 2023, Wiley-VCH.

active reactive species and further enhancing both electrocatalytic activity and stability for the OER.

3.2. Characterizations of the built-in electric field

By analyzing the electronic structure/valence state changes of various elements at the heterogeneous interface through XPS, XAFS, and EELS, the direction of electron transfer can be determined.[72] Meanwhile, the valence band energy levels can be calculated using XPS. The work function and band gap are measured using UPS and UV/vis DRS, respectively. By combining the valence band results obtained from XPS and the band gap results obtained from UV/vis DRS, the relative positions of the valence band and conduction band can be deduced. Subsequently, a corresponding energy level diagram is established to obtain the work function and Fermi level, which are used for preliminary judgment of the direction and strength of the BIEF.[73] EIS is used to obtain the Mott–Schottky plot and determine the type of semiconductor, thereby assessing the flat band potential. The band gap value from UV-vis DRS can determine the energy levels. In the solid-state *I–V* curve, the current of the composite material AB is higher than that of the single material A or single material B, and the inflection point potential of AB is more positive than that of A and B, indicating the presence of charge redistribution.[74,75] We have combined the XPS, UV/vis DRS, and EIS to characterize the BIEF present between the phosphide heterojunction.[70]

3.3. Strategies for tailoring built-in electric fields

The work function of the catalyst is a key factor determining the strength of the BIEF and the direction of charge transfer. Research has found that the main factors affecting the work function of the support include chemical valence state, surface defects, adsorbed atoms, and step density.[76–78] By regulating these factors, precise control of the work function of the support can be achieved. For example, Chen *et al.* reported a strategy of doping Mn into the Co_3O_4@NiFe-LDH p–n heterojunction to construct and reinforce the BIEF, aiming to elucidate the relationship between OER activity and the BIEF, as well as its intensity (Fig. 6a and b).[79] The BIEF generated by the p–n heterojunction effectively regulates the electronic structure, promotes electron transfer, induces changes in the chemical microenvironment, and adjusts the adsorption energy of intermediates (Fig. 6c and d). When the heteroatom Mn is introduced into the p–n heterojunction, particularly when doped into the NiFe-LDH with n-type semiconductor properties, a significant enhancement of the BIEF can be observed. DFT calculations further confirm that the construction and enhancement of the BIEF can effectively accelerate the electron transfer rate, regulate the d-band center, optimize the adsorption properties of intermediates, and reduce the reaction energy barrier (Fig. 6e and f).

Huang and coworkers also demonstrated that the creation of oxygen vacancies could tailor the work function of catalyst and thus regulate the intensity of the BIEF.[80] To be specific, they synthesized the $FeCo_2S_4$@O_v-CoFe-MOF/NF with rich oxygen vacancies. It is worth noting that the oxygen vacancies can increase the energy level difference of the two components and decrease the electron cloud overlap between the metal and oxygen for increased BIEF (Fig. 7a). As a result, such enhanced BIEF can accelerate the electron transport for optimizing the d-band center and the adsorption/desorption of intermediates (Fig. 7b).

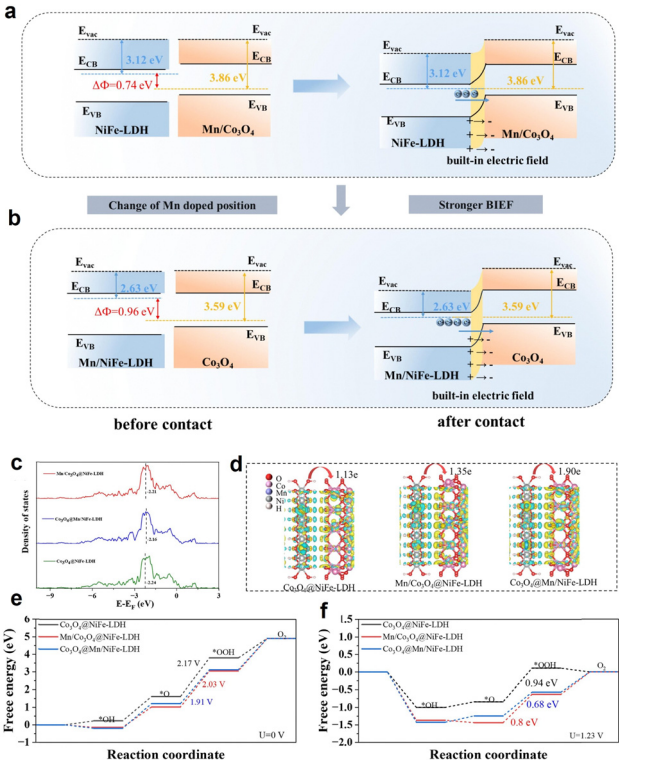

Fig. 6 (a) and (b) Schematic diagram of the electron transfer mechanism. (c) DOS diagram and d-band center of Ni for the different samples. (d) The charge density of various catalysts. The calculated free energy diagram of the OER on the active site (e) at U = 0 V and (f) U = 1.23 V. Reproduced with permission of ref. 79 copyright 2024, Elsevier.

4. Reconstruction of OER electrocatalysts *via* tailoring the built-in electric field

4.1. Reconstruction of metal oxide/hydroxide electrocatalysts *via* tailoring the built-in electric field

4.1.1. Importance of guiding reconstruction of metal oxide/hydroxide electrocatalysts. Metal oxide/hydroxide electrocatalysts have been widely investigated as electrocatalysts for the OER due to their unique electronic structure, appropriate adsorption with intermediates, and low cost.[81–83] More importantly, it is also demonstrated that most of the metal oxides/hydroxides will commonly undergo a typical dynamic reconstruction process to yield the highly active oxyhydroxides.[84] To guide the dynamic reconstruction process of metal oxides and hydroxides, enormous endeavors have been devoted and some effective strategies have been proposed.

4.1.2. Tailoring the BIEF for guiding the reconstruction of metal oxide/hydroxide electrocatalysts. Among them, the design

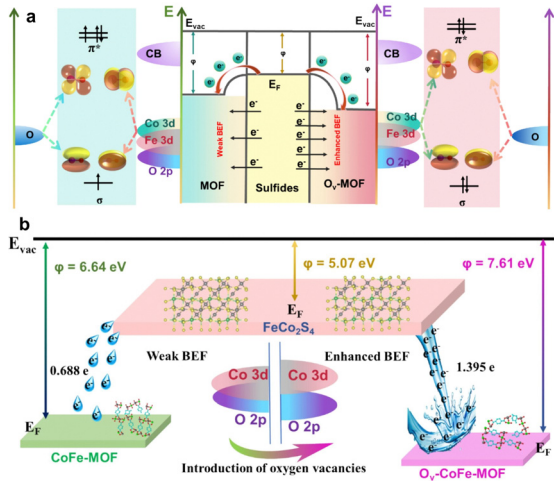

Fig. 7 (a) Schematic illustration of the BIEF-driven electron orbital coupling. (b) Schematically showing the regulation of BIEF intensity *via* introducing oxygen vacancies. Reproduced with permission of ref. 80 copyright 2024, Elsevier.

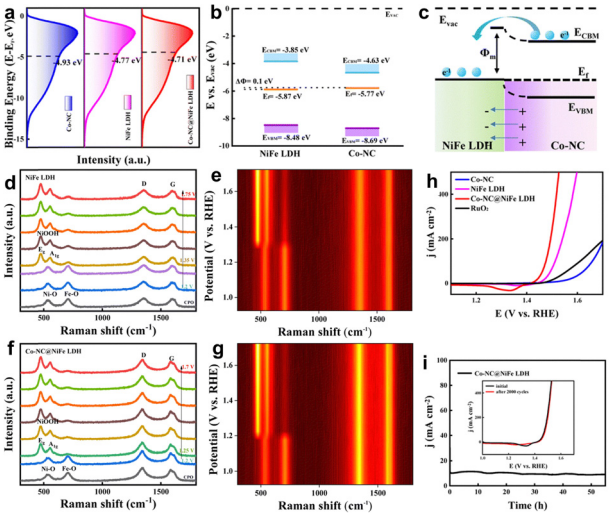

Fig. 8 (a) Surface valence-band spectra. (b) Energy band diagram. (c) Schematic diagram of the band structures. *In situ* Raman spectra of (d) and (e) NiFe LDH and (f) and (g) Co-NC@NiFe LDH. (h) OER polarization curves and (i) potentiostatic tests. Reproduced with permission of ref. 86 copyright 2024, Royal Society Chemistry.

and construction of the BIEF have been revealed to be a highly favorable approach. The presence of a tailored BIEF can facilitate the dynamic reconstruction of metal oxides/hydroxides during electrochemical reactions.[85] Moreover, by controlling the BIEF, it is possible to slow down undesirable processes such as dissolution or degradation of the electrocatalyst, thereby improving its operational stability during prolonged use. Furthermore, tailoring the BIEF can create asymmetric electron distributions, which can enhance charge transfer processes. This is particularly beneficial in electrocatalytic reactions, where efficient electron transfer is crucial. Thus, creating and tailoring the BIEF will benefit for guiding the dynamic reconstruction of metal oxides/hydroxides and further elevate their OER activity and stability.

4.1.3. Representative examples of tailoring the BIEF for guiding the reconstruction of metal oxide/hydroxide electrocatalysts. For example, Song *et al.* developed an N-doped carbon-supported Co and NiFe LDH (Co-NC@NiFe LDH) array, which could deliver superb OER and urea oxidation reaction (UOR) performance.[86] According to the energy band diagram and the *operando* characterizations, it is unveiled that the BIEF will serve as a driving force for charge flow from Co-NC to NiFe LDH, which not only boosts the electron redistribution to optimize the adsorption process of intermediates (Fig. 8a–c) but also facilitates the dynamic reconstruction of NiFe LDH into highly active hydroxyl oxides (Fig. 8d–g), thereby greatly augmenting the catalytic activity and stability (Fig. 8h and i). This work demonstrates that the construction of a BIEF into LDHs could not only optimize the adsorption energy with intermediates, but also guide the reconstruction process, which has emerged as a potential way to elevate the OER performance of catalysts.

4.2. Reconstruction of metal sulfide electrocatalysts *via* tailoring built-in electric fields

4.2.1. Importance of guiding reconstruction of metal sulfide electrocatalysts. Transition metal sulfides have become a hot topic in electrocatalysis in recent years due to their high intrinsic activity and excellent conductivity, making them one of the candidates for alkaline OER industrial catalysts.[87] The dynamic reconstruction phenomenon of metal sulfides during the electrocatalytic OER seriously hinders the in-depth study of phase transition mechanisms and the origin of electrocatalytic activity. Although previous research has demonstrated that the metal sulfides will undergo a typical reconstructing process to yield the highly active (oxy)hydroxides under OER conditions,[88] it is still a forbidden challenge to guide this process.

4.2.2. Tailoring the BIEF for guiding reconstruction of metal sulfide electrocatalysts. In recent years, the formation of BIEFs has been reported to be effective for inducing interfacial asymmetric distribution, rendering the formation of electron-rich and electron-deficient regions. In the electron-rich region of the BIEF, delocalized electrons create an electronic barrier for metal sites, which mitigates excessive losses during intense oxidation and redox reactions, thereby slowing down reconstruction processes. Therefore, rationally tailoring the intensity of the BIEF at metal sulfides will guide the reconstructing process.

4.2.3. Representative examples of tailoring the BIEF for guiding the reconstruction of metal sulfide electrocatalysts. For example, Zheng *et al.* proposed a BIEF strategy to assemble Co_9S_8/Ni_3S_2 heterojunctions confined in an S-doped carbon matrix (SC) and anchored S-doped carbide wood framework (SCW).[89] Electrochemical measurements demonstrated that such (Co_9S_8/Ni_3S_2)@SC/SCW could exhibit superb OER performance, with a low overpotential of 220 mV at 50 mA cm^{-2} (Fig. 9a). By combining experimental and theoretical investigations, it is uncovered that the BIEF can induce the directional transfer of electrons from Co_9S_8 to Ni_3S_2, which is favorable for the adsorption of OH^- because of the electrostatic interaction

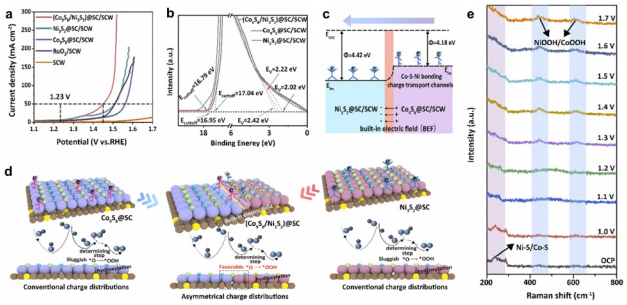

Fig. 9 (a) OER polarization curves of various catalysts. (b) UPS spectra of (Co_9S_8/Ni_3S_2)@SC/SCW and references. (c) Band distribution for Ni_3S_2@SC/SCW and Co_9S_8@SC/SCW. (d) Schematic illustration of the OER mechanisms catalyzed by (Co_9S_8/Ni_3S_2)@SC/SCW. (e) *In situ* Raman spectra of (Co_9S_8/Ni_3S_2)@SC/SCW monitored under OER conditions. Reproduced with permission of ref. 89 copyright 2025, Elsevier.

(Fig. 9b–d). Moreover, it is also unveiled that the electron-directed transport from Co_9S_8 to Ni_3S_2 can promote the surface dynamic reconstruction of (Co_9S_8/Ni_3S_2)@SC/SCW, leading to the formation of highly active amorphous metal oxyhydroxides (Fig. 9e). This study investigates the BIEF construction to promote the dynamic reconstruction of metal sulfides for achieving high OER performance.

4.3. Reconstruction of metal phosphide electrocatalysts *via* tailoring a built-in electric field

4.3.1. Importance of guiding reconstruction of metal phosphide electrocatalysts. Transition metal phosphides (TMPs) have received widespread attention due to their excellent electrical properties.[90] Due to the thermodynamic instability of phosphides in strongly oxidizing environments, the surface of phosphides used as pre-catalysts undergoes dynamic reconstruction, forming oxides or oxyhydroxides, which are essential for high OER activity.[91] Remarkably, exploring the surface evolution of electrocatalysts and identifying metastable intermediate states during the OER is crucial for revealing the true active sites and potential mechanisms. Recently, there has been great interest in introducing *in situ* tools to dynamically capture the evolution of catalyst structure or composition during operation.[92] In addition, it is also imperative to develop effective strategies to guide the dynamic reconstructing process of the TMPs. As previously mentioned, the creation of a BEIF can induce asymmetric charge distribution, which will benefit guiding the surface dynamic reconstruction of catalysts.[93]

4.3.2. Representative examples of tailoring the BIEF for guiding the reconstruction of metal phosphide electrocatalysts. Bearing this consideration in mind, tremendous efforts have been devoted to the design and fabrication of TMP heterostructures with a strong BIEF to achieve high OER performance. As a proof of concept, we have proposed an interfacial BIEF facilitated dynamic reconstruction strategy to improve the OER performance of TMP heterostructures.[94] To be specific, Xu *et al.* constructed an Fe_2P/NiCoP electrocatalyst with a robust BIEF through a MOF-mediated strategy. Detailed experiments demonstrated that the strong BIEF could facilitate the *in situ*

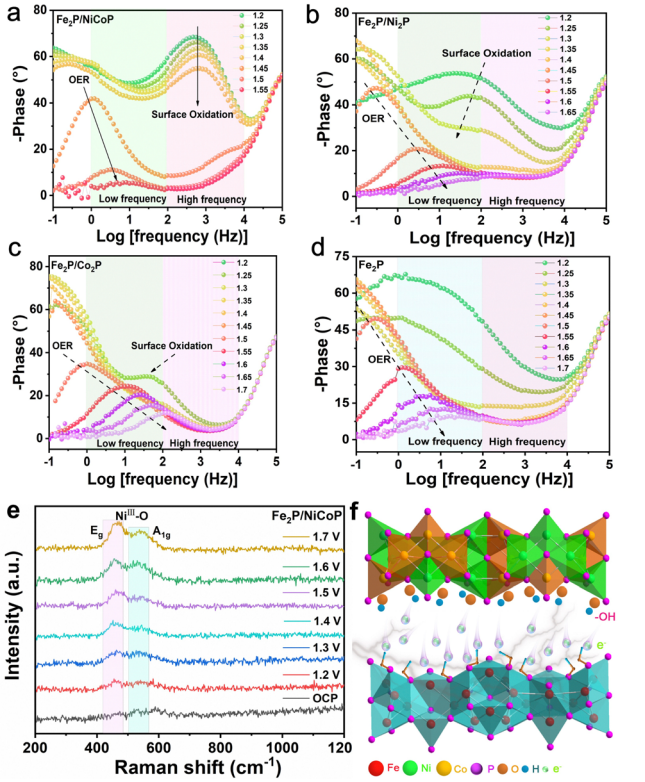

Fig. 10 Bode plots for (a) Fe_2P/NiCoP, (b) Fe_2P/Ni_2P, (c) Fe_2P/Co_2P, and (d) Fe_2P. (e) *Operando* Raman spectra of Fe_2P/NiCoP at different potentials. (f) Schematic diagram of the electron transfer in Fe_2P/NiCoP. Reproduced with permission of ref. 94 copyright 2024, Elsevier.

reconstruction of NiCoP into NiCoOOH, leading to a heterostructured catalyst with asymmetric charge distribution and thus endowing the Fe_2P with a positive surface charge (Fig. 10a–e). In addition to the formation of the highly active NiCoOOH, the robust BIEF could not only optimize the adsorption free energy, but also activate the Fe_2P to enhance the intrinsic activity (Fig. 10f). As a result, this heterostructure could deliver superb electrocatalytic OER performance, with the overpotentials of merely 247 and 255 mV to achieve 10 mA cm^{-2} in alkaline freshwater and simulated seawater, respectively. In conclusion, it is found that the creation of BIEF not only facilitates the dynamic reconstruction of metal phosphides to yield the highly active oxyhydroxides, but also reactivates the active sites to further elevate the OER performance.

4.4. Reconstruction of MOF electrocatalysts *via* tailoring the built-in electric field

4.4.1. Importance of guiding reconstruction of MOF electrocatalysts. MOFs show great promise for serving as the pre-catalysts for the OER, which include a high surface area, good tunability, and rich metal centers.[95] More importantly, the framework structure of MOFs has a high degree of dynamism and can undergo reconstruction under reaction conditions. This dynamic characteristic enables MOFs to adapt to different reaction environments, thereby generating more active species. During the reaction process, organic ligands in MOFs may

undergo desorption or recombination, forming new active sites. This change can significantly improve the efficiency of catalytic reactions, potentially affecting the catalytic activity and decreasing the electrochemical stability. Therefore, guiding the dynamic surface reconstruction of MOFs is crucial for achieving extraordinary OER activity and durability.

4.4.2. Representative examples of tailoring the BIEF for guiding the reconstruction of MOF electrocatalysts. It is acknowledged that the OER activity and dynamic reconstruction of catalysts are strongly correlated with the surface electronic state of catalysts. Therefore, tailoring the surface electronic state of MOF catalysts will be an effective and promising strategy for guiding their dynamic reconstruction process.[34] Inspired by the unique electron transport characteristics of the BIEF, it is necessary to introduce the BIEF into MOF-based heterostructures to induce asymmetric charge distribution. For example, Xu and coworkers have built a MIL-88B(Fe)@NiCo LDH heterojunction with a BIEF to guide its dynamic reconstruction.[96] It is demonstrated that a BIEF between MIL-88B(Fe) and NiCo LDH allows for a tunable work function difference. This configuration drives an asymmetric interfacial electron distribution, leading to electron accumulation at the Fe sites within MIL-88B(Fe) and creating electron-deficient LDHs (Fig. 11a and b). Consequently, this arrangement enhances the dynamic reconstruction of LDHs into oxyhydroxides while simultaneously mitigating the rapid dissolution of Fe during OER operations (Fig. 11c–e). Detailed electrochemical measurements revealed that such MIL-88B(Fe)@NiCo LDH could deliver extraordinary OER performance, with a remarkably low overpotential of 279 mV at 10 mA cm^{-2}, as well as outstanding electrochemical stability. Later, they have further introduced a unique polyaniline (PANI) electron bridge into the MOF and LDHs to expedite electron transfer from MOFs to LDHs, facilitating electron accumulation at the metal sites within the MOF and electron-deficient LDHs.[97] Profiting from the introduction of a PANI electron bridge (Fig. 11f), this configuration can further boost the dynamic reconstruction of LDHs into oxyhydroxides, while safeguarding the MOF from corrosion over long-term operation (Fig. 11g). Impressively, the overpotential at 10 mA cm^{-2} is remarkably decreased from 279 mV to 202 mV. These works have demonstrated that the creation of a BIEF can guide the reconstruction of MOFs to simultaneously maintain the high OER activity and durability.

BIEF-guided catalysts present a significant advancement in terms of potential efficiency improvements compared to traditional catalysts, especially in the electrocatalytic OER. As is well-known, BIEF-guided catalysts benefit from enhanced mass transport and a more favorable orientation of active sites due to the applied electric field. This results in improved reaction kinetics and potentially higher catalytic activity compared to traditional catalysts. The electric field can also help in selectively stabilizing certain reactive intermediates, leading to more efficient pathways during the OER. The traditional catalysts often rely on passive surface interactions and diffusion for reaction processes. Techniques such as electrocatalyst modification (*e.g.*, alloying or doping) can also enhance the efficiency,

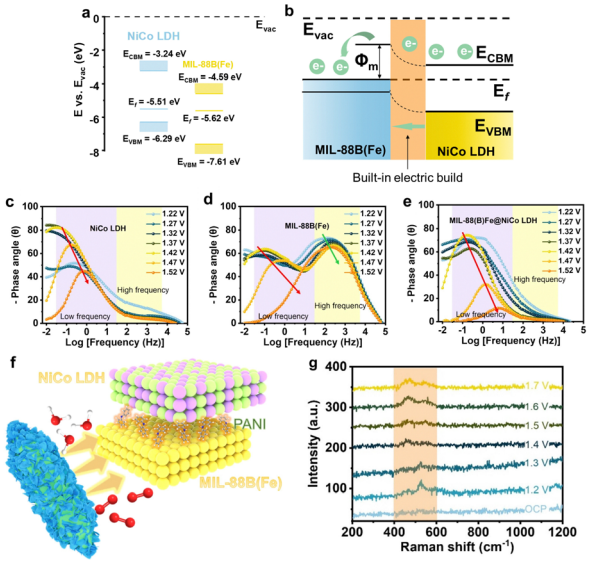

Fig. 11 (a) Energy-band alignment diagram of NiCo LDH and MIL-88B(Fe), and (b) schematic diagram of the band structures. The Bode phase plots of (c) NiCo LDH, (d) MIL-88B(Fe) and (e) MIL-88B(Fe)@NiCo LDH electrode. (f) Schematically illustrating the PANI electron bridge for accelerating the interfacial electron transfer within the MIL-88B(Fe)@NiCo LDH heterojunction. (g) *Operando* Raman spectra of MIL-88B(Fe)@PANI@NiCo LDH under different potentials. (a)–(e) Reproduced with permission of ref. 96 copyright 2024, Elsevier. (f) and (g) Reproduced with permission of ref. 97 copyright 2024, Elsevier.

but they may not achieve the same level of directivity and control afforded by BIEF.

In regard to the stability, one of the challenges faced by these catalysts is long-term stability, particularly in harsh environments (like acidic electrolytes). The electric field might lead to undesired side reactions or promote corrosion of the catalyst if not carefully controlled. However, if optimized, they can be designed to minimize degradation and maintain performance over time. Traditional catalysts like noble metals generally exhibit good stability in a variety of environments, especially in neutral or slightly basic conditions. However, in highly acidic environments, even noble metals can suffer from corrosion, which can limit their long-term viability.

Furthermore, the scalability of these systems can be challenging. Implementing the necessary electric field control in large-scale applications may require sophisticated engineering and may increase costs. However, if a viable pathway is developed for integration into existing technologies, the scalability could be promising. The scalability of emerging techniques can vary widely. Some innovative approaches might not yet have demonstrated large-scale feasibility, while others, such as certain types of nanomaterials or advanced composites, may offer scalable solutions but at a potentially higher production cost.

5. Conclusion and outlook

The rapid development of *ex situ* and *in situ* characterization techniques has stimulated the study of dynamic reconstruction

of catalysts. How to guide the dynamic reconstruction of catalysts under OER conditions has been a hotspot in recent years. The integration of BIEFs into the design of OER electrocatalysts has emerged as a transformative strategy to enhance electrocatalytic performance. This review has highlighted the critical role of BIEFs in promoting electron transfer, inducing asymmetric charge distribution, and facilitating surface dynamic reconstruction during the OER. The advancements discussed herein demonstrate that tailored electric fields can significantly improve the stability and activity of catalysts, leading to enhanced efficiency and longevity.

Looking ahead, further research is needed to deepen our understanding of the mechanisms by which BIEFs impact surface reconstruction at the atomic level. Future studies should focus on optimizing the design of BIEFs through advanced materials engineering and characterization techniques. Additionally, exploring the interplay between BIEFs and other external factors, such as temperature and the pH of the electrolyte, could yield valuable insights into the operational conditions that maximize electrocatalytic performance.

Moreover, the scalability of BIEF-engineered catalysts for practical applications remains a crucial area for exploration. Developing cost-effective synthesis methods and integrating these catalysts into real-world energy conversion systems will be essential for their commercial viability. As the demand for sustainable energy solutions continues to grow, the insights gained from this research will be pivotal in guiding the development of next generation electrocatalysts, ultimately contributing to more efficient and sustainable energy conversion technologies.

Most BIEF-guided reconstruction processes occur in alkaline electrolytes. Implementing BIEF-guided reconstruction in acidic electrolytes presents several potential challenges and limitations, including corrosion and stability issues, complex proton-catalyst interactions, formation of unstable intermediates, electric field distribution, compatibility with stability and performance metrics, and electrode material limitations. Therefore, it is essential to investigate the influence of the electrolyte on the reconstruction processes of OER electrocatalysts. Finding suitable materials that can both facilitate electric field-guided reconstruction and resist dissolution or degradation is key to advancing this technology.

BIEFs are generated at the interfaces of heterostructures, leading research on BIEF-guided reconstruction to primarily focus on heterostructured catalysts. However, in recent years, single-atom catalysts (SACs) have gained significant attention. The BIEF generated between different single atoms may also influence the performance of these catalysts. Therefore, it is crucial to investigate the impact of BIEFs on the performance and reconstruction of OER catalysts at the atomic level.

Data availability

No primary research results, software or code have been included and no new data were generated or analysed as part of this review.

Conflicts of interest

There are no conflicts to declare.

Acknowledgements

This work is supported by the financial support from the National Natural Science Foundation of China (No. 22305025, 22202169) and the Natural Science Foundation of Jiangsu Province (BK20230640).

Notes and references

1 H. Wang, J. Li, K. Li, Y. Lin, J. Chen, L. Gao, V. Nicolosi, X. Xiao and J.-M. Lee, *Chem. Soc. Rev.*, 2021, **50**, 1354–1390.
2 A. I. Zannah, I. Ferhoune, A. M. Abubakar, A. M. Al-Khudafi, A. A. Bitrus and W. Danladi, *Arch. Adv. Eng. Sci.*, 2023, **2**, 53–63.
3 H. Xu, K. Wang, G. He and H. Chen, *J. Mater. Chem. A*, 2023, **11**, 17609–17615.
4 Z. Li, L. Sun, Y. Zhang, Y. Han, W. Zhuang, L. Tian and W. Tan, *Coord. Chem. Rev.*, 2024, **510**, 215737.
5 B. Singh, A. Singh, A. Yadav and A. Indra, *Coord. Chem. Rev.*, 2021, **447**, 214144.
6 Y. Yang, J. Lou, Y. Zhao, J. Wei, Y. Zhou, C. Zhang, M. Wu, Y. Zhang, Q. Wang, L. Wang, T. Yang and X. Song, *Chem. Eng. J.*, 2023, **477**, 146900.
7 H. Xu, J. Yuan, G. He and H. Chen, *Coord. Chem. Rev.*, 2023, **475**, 214869.
8 J. Du, F. Li and L. Sun, *Chem. Soc. Rev.*, 2021, **50**, 2663–2695.
9 H. Xu, Y. Zhao, Q. Wang, G. He and H. Chen, *Coord. Chem. Rev.*, 2022, **451**, 214261.
10 Q. Wang, Z. Zhang, C. Cai, M. Wang, Z. L. Zhao, M. Li, X. Huang, S. Han, H. Zhou, Z. Feng, L. Li, J. Li, H. Xu, J. S. Francisco and M. Gu, *J. Am. Chem. Soc.*, 2021, **143**, 13605–13615.
11 Y. Wen, P. Chen, L. Wang, S. Li, Z. Wang, J. Abed, X. Mao, Y. Min, C. T. Dinh, P. Luna, R. Huang, L. Zhang, L. Wang, L. Wang, R. J. Nielsen, H. Li, T. Zhuang, C. Ke, O. Voznyy, Y. Hu, Y. Li, W. A. Goddard, III, B. Zhang, H. Peng and E. H. Sargent, *J. Am. Chem. Soc.*, 2021, **143**, 6482–6490.
12 J. Bai, L. Cheng, S. Liu, H. Zhang, Y. Lian, Y. Deng, Q. Zhou, Y. Tang and Y. Su, *Appl. Surf. Sci.*, 2024, **642**, 158613.
13 L. Ouyang, X. He, Y. Sun, L. Zhang, D. Zhao, S. Sun, Y. Luo, D. Zheng, A. M. Asiri, Q. Liu, J. Zhao and X. Sun, *Inorg. Chem. Front.*, 2022, **9**, 6602–6607.
14 J. Wei, J. Lou, W. Hu, X. Song, H. Wang, Y. Yang, Y. Zhang, Z. Jiang, B. Mei, L. Wang, T. Yang, Q. Wang and X. Li, *Small*, 2024, **20**, e202308956.
15 T. Wei, W. Liu, S. Zhang, Q. Liu, J. Luo and X. Liu, *Chem. Commun.*, 2023, **59**, 442–445.
16 Y. Xu, T. Liu, K. Shi, H. Yu, K. Deng, Z. Wang, X. Li, L. Wang and H. Wang, *Chem. Commun.*, 2023, **59**, 1817–1820.
17 Q. Zhou, Z. Qi, X. Yang, S. Pan, Y. Hu, A. L. Vasiliev, X. Wang and Y. Fu, *Ind. Eng. Chem. Res.*, 2024, **63**, 8142–8150.
18 H. Xu, Y. Liu, K. Wang, L. Jin, J. Chen, G. He and H. Chen, *Inorg. Chem.*, 2024, **63**, 16037–16046.
19 X. Luo, X. Tan, P. Ji, L. Chen, J. Yu and S. Mu, *EnergyChem*, 2023, **5**, 10091.
20 M. Zhao, J. Wang, C. Wang, Y. Sun, P. Liu, X. Du, H. Pan, H. Li, H. Liang, J. Guo and T. Ma, *Nano Energy*, 2024, **129**, 110020.
21 Z. Lu, J. Wang, P. Zhang, W. Guo, Y. Shen, P. Liu, J. Ji, H. Du, M. Zhao, H. Liang and J. Guo, *Appl. Catal., B*, 2024, **353**, 124073.
22 H. Zhong, Q. Zhang, J. Yu, X. Zhang, C. Wu, Y. Ma, H. An, H. Wang, J. Zhang, X. Wang and J. Xue, *Adv. Energy Mater.*, 2023, **13**, e2301391.
23 Y. Zhou, B. Chu, Z. Sun, L. Dong, F. Wang, B. Li, M. Fan and Z. Chen, *Appl. Catal., B*, 2023, **323**, 122168.
24 C. Fan, X. Wu, M. Li, X. Wang, Y. Zhu, G. Fu, T. Ma and Y. Tang, *Chem. Eng. J.*, 2022, **431**, 133829.
25 X. Li, C. Wang, S. Zheng, H. Xue, Q. Xu, P. Braunstein and H. Pang, *J. Colloid Interface Sci.*, 2022, **624**, 443–449.

26 H. Man, J. Feng, S. Wang, S. Li, P. Li, H. He, W. Raróg-Pilecka, J. Zhao, J. Zhang, F. Fang, D. Sun, Y. Li and Y. Song, *Cell Rep. Phys. Sci.*, 2022, **3**, 101059.
27 L. Zhang, J. Wang, K. Jiang, Z. Xiao, Y. Gao, S. Lin and B. Chen, *Angew. Chem., Int. Ed.*, 2022, **61**, e202214794.
28 Q. Mao, K. Deng, H. Yu, Y. Xu, Z. Wang, X. Li, L. Wang and H. Wang, *Adv. Funct. Mater.*, 2022, **32**, e2201081.
29 J. Zhao, J. Lian, Z. Zhao, X. Wang and J. Zhang, *Nano-Micro Lett.*, 2022, **15**, 19.
30 X. Zhang, H. Yi, M. Jin, Q. Lian, Y. Huang, Z. Ai, R. Huang, Z. Zuo, C. Tang, A. Amini, F. Jia, S. Song and C. Cheng, *Small*, 2022, **18**, e2203710.
31 W. H. Lee, M. H. Han, Y.-J. Ko, B. K. Min, K. H. Chae and H.-S. Oh, *Nat. Commun.*, 2022, **13**, 605.
32 J. Sun, H. Xue, N. Guo, T. Song, Y. R. Hao, J. Sun, J. Zhang and Q. Wang, *Angew. Chem., Int. Ed.*, 2021, **60**, 19435–19441.
33 Y. Yi, Q. Wu, J. Li, W. Yao and C. Cui, *ACS Appl. Mater. Interfaces*, 2021, **13**, 17439–17449.
34 H. Chen, Z. Yu, Y. Hou, R. Jiang, J. Huang, W. Tang, Z. Cao, B. Yang, C. Liu and H. Song, *Nanoscale*, 2021, **13**, 20670–20682.
35 T. Zhao, C. Liu, F. Yi, W. Deng, A. Gao, D. Shu and L. Zheng, *Electrochim. Acta*, 2020, **364**, 137260.
36 W. J. Sun, H. Q. Ji, L. X. Li, H. Y. Zhang, Z. K. Wang, J. H. He and J. M. Lu, *Angew. Chem., Int. Ed.*, 2021, **60**, 22933–22939.
37 Z. Li, Y. Pei, R. Ma, Y. Wang, Y. Zhu, M. Yang and J. Wang, *J. Mater. Chem. A*, 2021, **9**, 13109–13114.
38 H. Chu, D. Zhang, P. Feng, Y. Gu, P. Chen, K. Pan, H. Xie and M. Yang, *Nanoscale*, 2021, **13**, 19518–19526.
39 C. Xue, H. An, G. Shao and G. Yang, *Chin. J. Catal.*, 2021, **42**, 583–594.
40 H. Yang, B. Wang, S. Kou, G. Lu and Z. Liu, *Chem. Eng. J.*, 2021, **425**, 131589.
41 D. Chen, R. Lu, R. Yu, Y. Dai, H. Zhao, D. Wu, P. Wang, J. Zhu, Z. Pu, L. Chen, J. Yu and S. Mu, *Angew. Chem., Int. Ed.*, 2022, **61**, e202208642.
42 L. Zhai, X. She, L. Zhuang, Y. Li, R. Ding, X. Guo, Y. Zhang, Y. Zhu, K. Xu, H. J. Fan and S. P. Lau, *Angew. Chem., Int. Ed.*, 2022, **61**, e202116057.
43 J. Liu, W. Du, S. Guo, J. Pan, J. Hu and X. Xu, *Adv. Sci.*, 2023, **10**, e2300717.
44 Y. Zeng, M. Zhao, Z. Huang, W. Zhu, J. Zheng, Q. Jiang, Z. Wang and H. Liang, *Adv. Energy Mater.*, 2022, **12**, e2201713.
45 Y. Hu, Y. Zheng, J. Jin, Y. Wang, Y. Peng, J. Yin, W. Shen, Y. Hou, L. Zhu, L. An, M. Lu, P. Xi and C.-H. Yan, *Nat. Commun.*, 2023, **14**, 1949.
46 Y. Yuan, Q. Wang, Y. Qiao, X. Chen, Z. Yang, W. Lai, T. Chen, G. Zhang, H. Duan, M. Liu and H. Huang, *Adv. Energy Mater.*, 2022, **12**, e2200970.
47 Y. J. Wu, J. Yang, T. X. Tu, W. Q. Li, P. F. Zhang, Y. Zhou, J. F. Li, J. T. Li and S. G. Sun, *Angew. Chem., Int. Ed.*, 2021, **60**, 26829–26836.
48 H. Xu, K. Wang, L. Jin, L. Yang, J. Yuan, W. Zhang, G. He and H. Chen, *J. Colloid Interface Sci.*, 2023, **650**, 1500–1508.
49 Y. Chen, H. Li, J. Wang, Y. Du, S. Xi, Y. Sun, M. Sherburne, J. W. Ager, A. C. Fisher and Z. J. Xu, *Nat. Commun.*, 2019, **10**, 572.
50 J. Liu and L. Guo, *Matter*, 2021, **4**, 2850–2873.
51 Y. Cui, Z. Xu, D. Chen, T. Li, H. Yang, X. Mu, X. Gu, H. Zhou, S. Liu and S. Mu, *Nano Energy*, 2021, **90**, 106579.
52 Y. Pi, Y. Xu, L. Li, T. Sun, B. Huang, L. Bu, Y. Ma, Z. Hu, C. W. Pao and X. Huang, *Adv. Funct. Mater.*, 2020, **30**, e2004375.
53 X. Zheng, X. Shi, H. Ning, R. Yang, B. Lu, Q. Luo, S. Mao, L. Xi and Y. Wang, *Nat. Commun.*, 2023, **14**, 4089.
54 W. Shen, Y. Zheng, Y. Hu, J. Jin, Y. Hou, N. Zhang, L. An, P. Xi and C.-H. Yan, *J. Am. Chem. Soc.*, 2024, **146**, 5324–5332.
55 P. C. Chen, C. Chen, Y. Yang, A. L. Maulana, J. Jin, J. Feijoo and P. Yang, *J. Am. Chem. Soc.*, 2023, **145**, 10116–10125.
56 H. Q. Ta, R. G. Mendes, Y. Liu, X. Yang, J. Luo, A. Bachmatiuk, T. Gemming, M. Zeng, L. Fu, L. Liu and M. H. Rummeli, *Adv. Sci.*, 2021, **8**, e2100619.
57 J. Fan, J. Wu, X. Cui, L. Gu, Q. Zhang, F. Meng, B. H. Lei, D. J. Singh and W. Zheng, *J. Am. Chem. Soc.*, 2020, **142**, 3645–3651.
58 Y. Yao, G. Zhao, X. Guo, P. Xiong, Z. Xu, L. Zhang, C. Chen, C. Xu, T.-S. Wu, Y.-L. Soo, Z. Cui, M. M.-J. Li and Y. Zhu, *J. Am. Chem. Soc.*, 2024, **146**, 15219–15229.
59 L. Cao, X. Liu, X. Shen, D. Wu and T. Yao, *Acc. Chem. Res.*, 2022, **55**, 2594–2603.
60 X. Hu, Z. Xiao, W. Wang, L. Bu, Z. An, S. Liu, C. W. Pao, C. Zhan, Z. Hu, Z. Yang, Y. Wang and X. Huang, *J. Am. Chem. Soc.*, 2023, **145**, 15109–15117.
61 Y.-Z. Wang, J. Wang, X. Wang and B. Ren, *Curr. Opin. Electrochem.*, 2023, **42**, 101385.
62 Z. Xiao, Y.-C. Huang, C.-L. Dong, C. Xie, Z. Liu, S. Du, W. Chen, D. Yan, L. Tao, Z. Shu, G. Zhang, H. Duan, Y. Wang, Y. Zou, R. Chen and S. Wang, *J. Am. Chem. Soc.*, 2020, **142**, 12087–12095.
63 X. Liu, X. Duan, T. Bao, D. Hao, Z. Chen, W. Wei, D. Wang, S. Wang and B. J. Ni, *J. Hazard. Mater.*, 2022, **430**, 128195.
64 X. Zhao, M. Liu, Y. Wang, Y. Xiong, P. Yang, J. Qin, X. Xiong and Y. Lei, *ACS Nano*, 2022, **16**, 19959–19979.
65 X. Yang, Z. Zhang, Y. Zhang, W. Du, M. Ye, Y. Tang, Z. Wen, X. Liu and C. C. Li, *Energy Environ. Sci.*, 2024, **17**, 5102–5114.
66 H. Xu, Z. Xu, K. Wang, L. Jin, Y. Liu and L. Li, *Chem. Commun.*, 2024, **60**, 13507–13517.
67 Z. Wang and S. Wang, *Appl. Catal., B*, 2024, **352**, 124002.
68 X. Wang, X. Yu, P. He, G. Yang, F. Qin, Y. Yao and L. Ren, *Chem. Eng. J.*, 2024, **496**, 154279.
69 Z. Feng, F. Lu, Q. Hu, J. Qiu, X. Lei, B. Wang, R. Guo, Y. Tian, X. Liu and J. You, *J. Mater. Chem. A*, 2024, **12**, 18047–18070.
70 L. Jin, H. Xu, K. Wang, L. Yang, Y. Liu, X. Qian, G. He and H. Chen, *Appl. Surf. Sci.*, 2024, **657**, 159777.
71 S. Zhao, Y. Wang, Y. Hao, L. Yin, C. H. Kuo, H. Y. Chen, L. Li and S. Peng, *Adv. Mater.*, 2023, **35**, e2308925.
72 R.-Q. Li, Y.-J. Bian, C.-M. Yang, L. Guo, T.-X. Ma, C.-T. Wang, F. Fu and D.-J. Wang, *Rare Met.*, 2023, **43**, 1125–1138.
73 B. Tu, J. Hao, F. Wang, Y. Li, J. Li and J. Qiu, *Chem. Eng. J.*, 2023, **456**, 141103.
74 X. Chen, D. Shi, M. Bi, J. Song, Y. Qin, S. Du, B. Sun, C. Chen and D. Sun, *J. Colloid Interface Sci.*, 2023, **652**, 653–662.
75 X. H. Chen, J. Y. Ren, N. B. Li and H. Q. Luo, *J. Colloid Interface Sci.*, 2023, **651**, 760–768.
76 X. Qin, L. Ji and A. Zhu, *Appl. Surf. Sci.*, 2024, **652**, 159338.
77 T. Jiang, Y. Wang, Z. Guo, H. Luo, C. Zhan, Y. Wang, Z. Wang, F. Jiang and H. Chen, *J. Cleaner Prod.*, 2022, **341**, 130908.
78 W. He, L. Liu, T. Ma, H. Han, J. Zhu, Y. Liu, Z. Fang, Z. Yang and K. Guo, *Appl. Catal., B*, 2022, **306**, 121107.
79 J. Wu, X. Gao and Z. Chen, *Chem. Eng. J.*, 2024, **492**, 152241.
80 X. Hou, T. Ni, Z. Zhang, J. Zhou, S. Zhang, L. Chu, S. Dai, H. Wang and M. Huang, *Chem. Eng. J.*, 2024, **495**, 153464.
81 G. Fang, X. Ji, H. Shi, C. Zhang, Z. Guo, T. Tang and W. Liu, *J. Alloys Compds.*, 2024, **970**, 172583.
82 S. Fan, B. Zhu, Y. Zhong, S. Shi, J. Zhang and C. Chen, *Chem. Eng. J.*, 2023, **474**, 145905.
83 H. Li, Y. Sun, J. Wang, Y. Liu and C. Li, *Appl. Catal., B*, 2022, **307**, 121136.
84 J. Yuan, B. Huang, Y. Lu, H. Xu, Y. Qiao, H. Xu, G. He and H. Chen, *Appl. Surf. Sci.*, 2023, **610**, 155480.
85 P. Zhao, S. Fu, Y. Luo, C. Peng, L. Cheng and Z. Jiao, *Small*, 2023, **19**, e2305241.
86 T. Song, H. Xue, J. Sun, N. Guo, J. Sun, Y.-R. Hao and Q. Wang, *Chem. Commun.*, 2024, **60**, 972–975.
87 X. Liu, X. Zhao, S. Cao, M. Xu, Y. Wang, W. Xue and J. Li, *Appl. Catal., B*, 2023, **331**, 122715.
88 R. He, X. Huang and L. Feng, *Energy Fuels*, 2022, **36**, 6675–6694.
89 L. Zheng, H. Luo, Y. Zhong, W. Li, H. Xu, F. Xiong, J. Pi, Y. Qing and Y. Wu, *Appl. Catal., B*, 2025, **360**, 124550.
90 Y. Yang, R. Zou, J. Gan, Y. Wei, Z. Chen, X. Li, S. Admassie, Y. Liu and X. Peng, *Green Chem.*, 2023, **25**, 4104–4112.
91 H. Xu, L. Jin, K. Wang, L. Yang, G. He and H. Chen, *Int. J. Hydrogen Energy*, 2023, **48**, 38324–38334.
92 M. Xing, D. Zhang, D. Liu, C. Song and D. Wang, *J. Colloid Interface Sci.*, 2023, **629**, 451–460.
93 X. Zhang, Y. Dong, Q. Lv, F. wang, C. Jiang, Y. Wang, J. Dou, Q. Guo, B. Dong and Q. Tang, *Appl. Catal., B*, 2024, **342**, 123400.
94 H. Xu, L. Jin, K. Wang, L. Yang, Y. Liu, G. He and H. Chen, *Fuel*, 2024, **369**, 131716.
95 A. Kundu, T. Kuila, N. C. Murmu, P. Samanta and S. Das, *Mater. Horiz.*, 2023, **10**, 745–787.
96 H. Xu, L. Yang, Y. Liu, L. Jin, K. Wang, G. He and H. Chen, *Fuel*, 2024, **377**, 132796.
97 H. Xu, L. Yang, L. Jin, Y. Liu, K. Wang, J. Chen, G. He and H. Chen, *J. Colloid Interface Sci.*, 2025, **677**, 158–166.